Available online at www.dergipark.org.tr/en

INTERNATIONAL ADVANCED RESEARCHES and ENGINEERING JOURNAL

Journal homepage: www.dergipark.org.tr/en/pub/iarej

e-ISSN: 2618-575X

International Open Access

Volume 07
Issue 01

April, 2023

Research Article

Numerical investigation of aerodynamic performance and noise characteristic of air multiplier bladeless fan

Firdevs Yedekcioglu [a], ***Sumeyye Akyildiz*** [b] ***and Zekeriya Parlak*** [c,*]

[a]*Sakarya University, Institute of Natural Sciences, Sakarya 54187,Turkiye*
[b]*Gazi University, Graduate School of Natural and Applied Science, 06560, Teknikokullar, Ankara, Turkiye*
[c]*Sakarya University, Department of Mechanical Engineering, Sakarya 54187,Turkiye*

ARTICLE INFO

Article history:
Received 26 July 2022
Accepted 03 February 2023
Published 15 April 2023

Keywords:
Acoustic
Air Multiplier Fan
CFD
EPPLER
NACA
Noise

ABSTRACT

Air multiplier fans, which are produced as an alternative to the convectional propellers used today, have come into prominence with the advantages providing in both efficiency and usage. In this study, three different blade profiles based on NACA 0012, NACA 1408, and EPPLER 1214 were used in the fan body. The design based on the NACA 0012 of body profile provided the highest flow rate. This profile was optimized using CFD analysis according to seven different geometrical parameters determined as the angle of attack, width, length, gap, inner and outer diameters, and tail length. The profile that provides less noise against the highest flow rate was determined as the optimal design. With CFD analysis, the sound pressure level of the optimal design was calculated by the k-ω and LES method, and the results were compared with each other.

1. Introduction

Today, while designing the fan, new and special designs are made by trying to improve the features of the fan. Despite the fact that fans are typically divided into axial or radial, the bladeless mechanism is distinct from both, this novel fan was developed by the English company Dyson in 2009 as an alternative to conventional fans. This fan design has become remarkable due to the simple shape of the model, the absence of a visible rotating fan, stable air supply, portability, easy cleaning, and reliability for children and pets. The device called as bladeless fan or air multiplier consists of two parts the cylindrical lower part and the circular air frame [1]. As shown in Figure 1, the air is sucked in by the fan in the body, accelerated, and forced to pass through the circular narrowing gap under high pressure at the back of the frame. According to Bernoulli's equation, the air accelerates while the passing through the narrowing slit and pressure drops [2].

Initially, it dwelled on the practical applications, social and economic implications of the air multiplier rather than its theoretical research. Li et al. [3] examined the effect the Coanda surface in the different curvatures on the performance of the air multiplier. They designed and simulated 5 types of Coanda surfaces with different curvatures and compared the results with the prototype. Lasse and Simon [4] analyzed the flow characteristics of the Dyson air multiplier, performed CFD analysis for two different turbulence models, k-ε and k-ω, and determined that the k-ε turbulence model produced more accurate results for the air multiplier fan. Li et al. [5] investigated the outlet flow field of the air multiplier numerically and experimentally, analyzed it according to the k-ε model and confirmed the results with CTA, and concluded that the RNG k-ε model is a reliable model for estimating the time-dependent flow cycle in the fan outlet area.

Jafari et al. [6] investigated the potential of using a bladeless fan of 60 cm diameter inside a cubic room for industrial applications with numerical analysis and also examined its performance with experimental tests. According to the results of this study, the bladeless air multiplier can be designed in large sizes and used in a variety of industries such as underground tunnels or to remove smoke and dust from industrial environments.

Zafer and Gürsoy [7] in this study is concerned with the computational aero-acoustic analysis of an airfoil with jet blowing. The airfoil shape is chosen as NACA0015 profile with jet blowing on upper surface. The calculations of analysis are done by using commercial finite volume solver. The k-ε turbulence model is used for the turbulence modeling and the Ffowcs Williams and Hawking acoustic

* Corresponding author. Tel.: *+90 264 295 5495.*
E-mail addresses: firdevs.yedekcioglu@gmail.com *(F. Yedekcioglu)*, sumeyye.akyildiz@gazi.edu.tr *(S. Akyildiz)*, zparlak@sakarya.edu.tr *(Z. Parlak)*
ORCID: 0000-0002-7471-2495 *(F. Yedekcioglu)*, 0000-0002-8166-2254 *(S. Akyildiz)*, 0000-0002-2487-0065 *(Z. Parlak)*
DOI: 10.35860/iarej.1148880

analogy model is run for determination of acoustic data. The numerical results are compared with experimental data for computed Sound Pressure Level without jet blowing and well agreement is observed. The effects of different jet angles, velocity ratios, and angles of attack on airfoil are investigated in the case of jet blowing, and noise levels of non-jet and jet blowing cases are studied.

Kocak at al. [8] in this investigation flow performance of the rod-airfoil configurations is taken into consideration in order to understand the flow physics and acoustic performance of turbomachines, such as fans, wind and water turbines. Shear layer and Von-Karman vortex structures break apart at the leading edge of the airfoil and small vortices are generated through the airfoil. Due to the flow-solid surface interaction, noise and vibration arise. Rod-airfoil configurations can perfectly model turbomachines because the main cause of broadband noise in turbomachines is also incoming turbulent and stator interaction. The airfoil is placed in the wake region of the cylinder and the obtained results are compared with the experimental results from the literature. It was shown that, the developed numerical method and Computational Aeroacoustics Analysis (CAA) methodology compare well with the measurements obtained in an accompanying experiment. After validating, the results obtained with the developed numerical methodology, the cylinder diameter effects on vortex zones, separation point, reattachment point and sound pressure level is investigated. It was observed that with the increase in the Strouhal number, the Sound Pressure Level (SPL) levels of the configuration rises.

İlter [9] computed the flow around NACA 0012 foil using numerical techniques, and the effects of edge angle of attack and trailing edge shape on flow noise were investigated in two dimensions. In order to validate this study, the flow noise around a circular cylinder has also been investigated. The pressure fluctuations around the body were obtained by numerically solving Navier Stokes equations, and the equations were discretized using the Finite Volume Method (FVM), which is widely used in fluid dynamics The quadrupole component of sound was investigated by using Curle and Proudman methods which were derived from Lighthill analogy and far field noise was computed by using Ffowcs Williams and Hawkings (FW-H) equations.

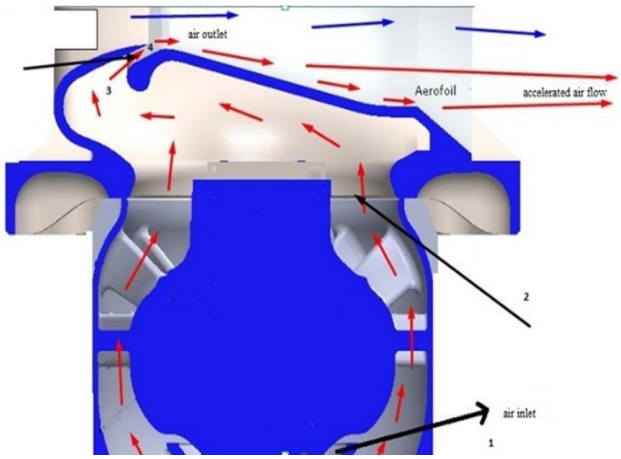

Figure 1. Working Principle of Fan

The sound pressure levels of an axial fan are numerically investigated in this paper using the Ffowcs-Williams & Hawkings (FW-H) analogy and the computational fluid dynamics (CFD) method. A simulation model based on unstructured mesh structure and Standard k-epsilon (k-ε) turbulence model is established for high speed rotation (3000 RPM), and the numerical simulation results are compared with experimental data specified by blade manufacturer company. Noise generation mechanism in the axial fan shroud are discussed using with the numerical results. [10]

Li [11] created and studied a bladeless fan prototype using numerical simulations in the current study. The entire fan prototype, including wind channel, base, rotor, and stator, is used to characterize the aerodynamic and aeroacoustic performances of the bladeless fan; when investigating the influence of the wind channel's geometric parameters, only the wind channel is considered in simulations. The effects of slit width, cross-section height, slit location, and cross-section profile are investigated.

Mehmood et al. [12] computationally analyzed a circular type bladeless ceiling fan in a standard empty room (4m x 4m x 4m). Different design features such as fan radius, height from the ceiling and floor, fan jet width, mass flow rate, and orientations were studied metrically, and their effect on perceived comfort level in terms of velocity spread and average velocities was computed. The results show that the fan height in the close vicinity of ceiling does not affect the flow field in the occupied zones, however, as the fan gets closer to the floor the velocity field in the occupied zone changes due to creation of a strong vortex at the center of floor. Thus, fan installation closer to the ceiling (less than 0.5m from the ceiling) is a preferred choice. With an increase in fan radius from 0.3m to 0.5m, an increment of 33% was observed in velocity spread thus increasing the zone of influence.

Ravi and Rajagopal. [13] conducted a three-dimensional numerical study to investigate the effect of various geometric shapes and slit angles on bladeless fan performance for various aerodynamic profiles. Airfoils considered for the present study are E169, E473 and E479 which are then reformed into a typical bladeless fan arrangement. The three-dimensional fluid flow variations through and across the airfoil were simulated by solving the governing equations, namely the continuity and Reynolds Averaged Navier-Stokes equations (RANS). The three-dimensional fluid flow variations through and across the airfoil have been simulated by solving the appropriate governing equations namely continuity and Reynolds Averaged Navier-Stokes equations (RANS). Numerically predicted results of lift, drag and streamwise velocity decay along the jet centerline of a cylindrical channel are compared with literature and a very close agreement exists between the two. Upon validation, geometric shapes - circular and square cross section with aspect ratios of 1, 1.5 and 2 and slit angles of 20, 40, 60 and 80 degrsee for all the above three airfoil configurations are analyzed numerically for various inlet Reynolds number. From the study it is observed that Eppler 473 airfoil profile

with slit thickness of 1 mm and slit angle of 80° provided the maximum discharge ratio of 34.17 for an inlet mass flow rate of 80 LPS.

Jafari et al [14] investigated effect of five geometric parameters on well aeroacoustic sound performance of a Bladeless fan. Li et al [15] investigated the outlet flow field of an annular jet for a bladeless fan experimentally using constant temperature anemometer hot-wire system at five Reynolds numbers. Joshi et al [16] investigated the influence of the airfoil's outlet slit thickness on the discharge ratio by varying the outlet slit thickness of an Eppler 473 airfoil from 1.2 mm to 2 mm in intervals of 0.2 mm. Results indicated that smaller slits showed higher discharge ratios.

In this study, three different bladeless fan geometries were created based on NACA 0012, NACA 1408 and EPPLER 1214 airfoils. As a result of CFD analysis, NACA 0012 was chosen because it gave the highest flow rate. The optimization study was made in the ANSYS Response Surface Optimization module according to seven different geometrical design parameters for the NACA 0012 profile to obtain the least noise against the best flow rate. The optimal geometry of the circular airfoil profile was determined as a result of the optimization by CFD analyses. Also, the sound pressure levels of the bladeless fan were calculated with both k-ω and the LES method and the results were compared with each other.

2. Design and CFD Analysis

Figure 2 shows the airflow in the propeller geometry of air multiplier manufactured by Dyson. Air, which is forced pass through the circular narrow gap at high velocity and low pressure, causes that air behind into the device also sucks towards the circular frame with the Coanda effect, thus total flow rate becomes a lot of times increased, it is defined as the multiplied flow rate. The ratio of the flow rate coming out of the airfoil circular body and the flow rate suctioned the inlet pipe by the rotating fan can be defined as follows.

$$Q_{inlet} = V_{inlet} \times A_{inlet} \quad (1)$$

However, Dyson company stated that this ratio is about 15.

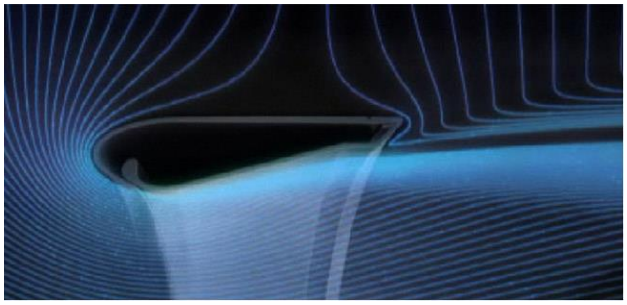

Figure 2. The effect of the Coanda effect on the air multiplier propeller [2]

Lasse and Simon [4] analyzed the device with a bladeless profile section without a bottom cylinder. Thermophysical properties of the air are accepted as density (ρ) is 1.225 kg/m^3, dynamic viscosity (μ) is 1.7894.10-5 kg/ms airflow velocity (V) is 2.5 m/s. They stated that the fan generates less noise due to low turbulence generation, there is some high turbulence near the jet nozzle, the output current is relatively constant.

Three different geometries were created for the same parameters based on three different airfoils, which are NACA0012, NACA1408 and EPPLER1214. Among these profiles, NACA0012 was chosen because it is generally used in the literature, NACA1408 was chosen because it is similar to the NACA 0012 profile as symmetrical characteristic. EPPLER1214 model was chosen as an alternative model. The determined airfoils are given in Figure 3.

The model shown in Figure 4 was drawn in the ANSYS DesignModeller tool. The system consists of two units. The lower unit is the section where the air enters and the second unit is the section through which the air is directed and sent from a circular narrow gap. The view of the airfoil on the geometry is shown in Figure 4. The mesh is shown in Figure 5. The skewness value of the mesh is greater than 0.7, however the number of elements with these skewness values is extremely low. The same is valid for orthogonal quality values less than 0.2. Because it has a very complex geometry and extremely small gaps through which the fluid passes, the best available mesh has been developed after mesh independence tests.

For the turbulence model, a solution was tried by both k-ε and k-ω and the analyzes were continued with k-ω since better convergence. In order to capture the boundary layer correctly, the mesh density in the boundary layer was determined for the y+ value, which was obtained about as 1 and maximum 1.8 for all three profiles.

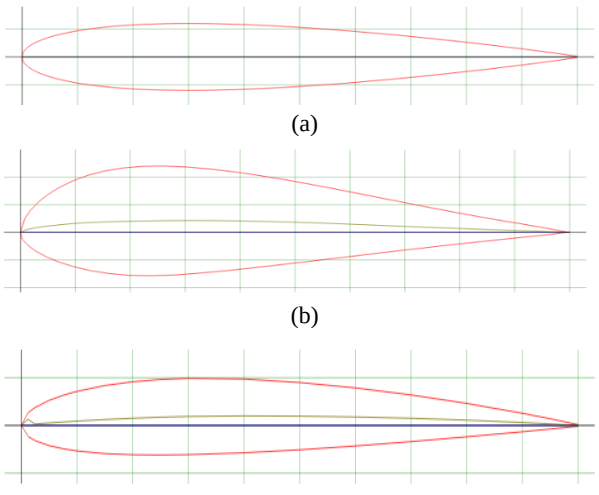

(a) (b) (c)

Figure 3. Chosen airfoiller (a) NACA0012, (b) NACA1408 and (c) EPPLER1214

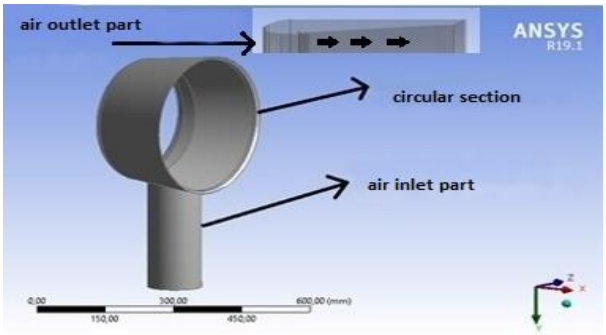

Figure 4. Geometry model based on NACA 0012 airfoil.

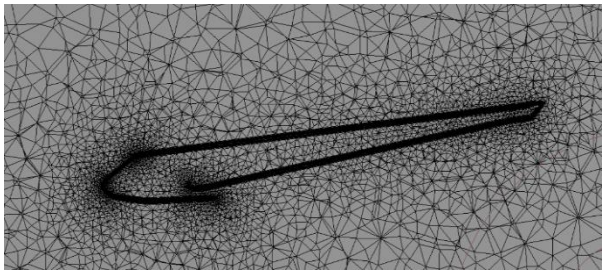

Figure 5. Mesh (NACA 0012)

3. Results of Aerodynamic Analysis

Boundary conditions for aerodynamic analysis of bladeless fan are shown in Table 1. The design parameters are shown in Table 2. and Figure 6.

Table 1. Boundary Conditions

Velocity inlet	Outlet pressure	Turbulence model
0.02 m^3/s	0 Pa	k-ω

Table 2. Initial values of design parameters

Parameter	Initial Values
Width [mm]	9
The angle of Attack [°]	7
Gap [mm]	5
Diameter [mm]	116
Tail Length [mm]	10
Tail Angle [°]	45
Length [mm]	200

When the velocity vectors in Figure 7 and the velocity contours in Figure 8 are examined for the three airfoil geometries, it is seen that the circular airfoil geometry designed based on the NACA0012 profile accelerates the airflow more than the others. While the maximum velocity is approximately 18 m/s in the NACA 0012 profile, it is calculated as 12.5 m/s in the NACA1408 profile and 12 m/s in the EPPLER1214 profile. In addition, the flow is more stable and homogeneous in the NACA0012 profile. Due to the airfoil structure, the flow is more turbulent in the NACA1408 profile.

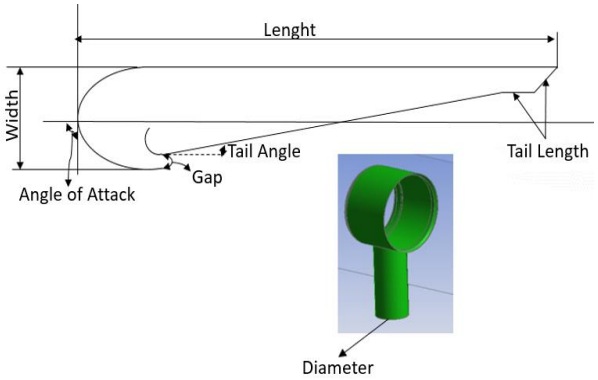

Figure 6. Design parameters determined for analysis in NACA 0012 airfoil geometry

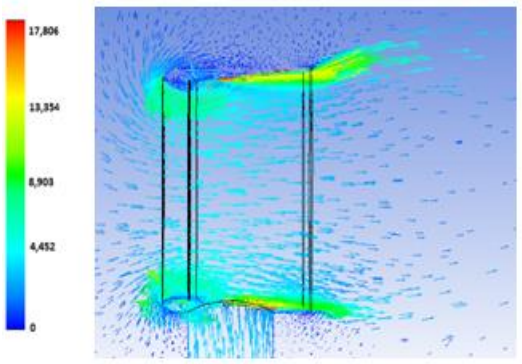

(a)

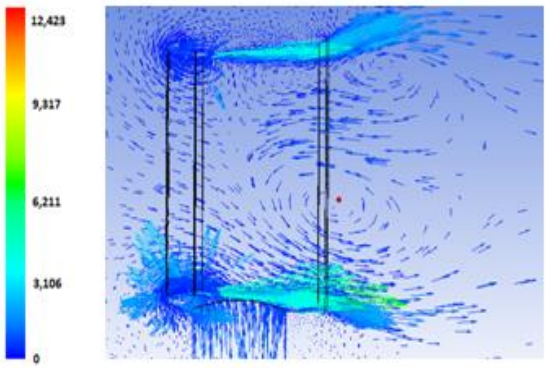

(b)

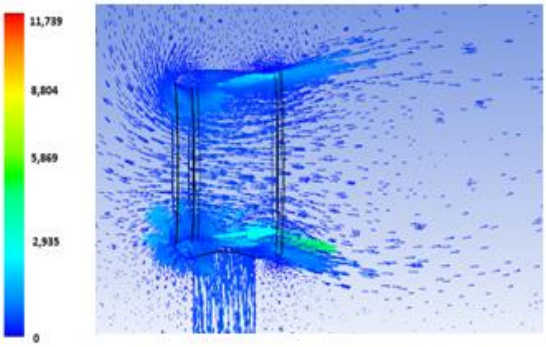

(c)

Figure 7. a) Velocity vectors of a) NACA0012, b) NACA1408, c) EPPLER 1214 profiles

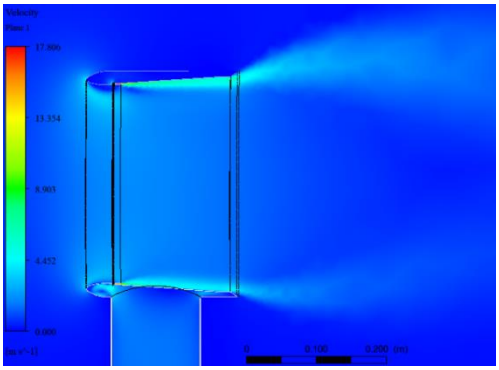

(a)

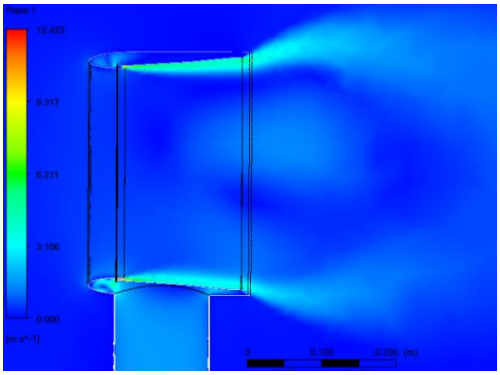

(b)

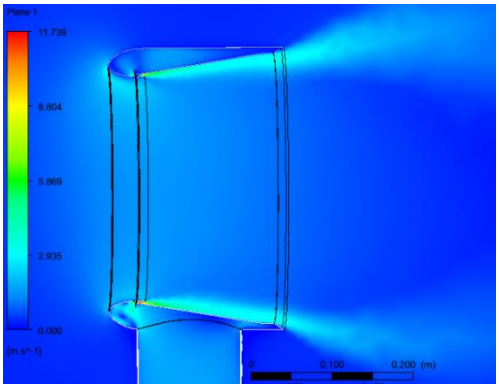

(c)

Figure 8. a) NACA 0012, b) NACA 1408, c) EPPLER 1214 velocity contours for shell design

The ratios of the flow rate at outlet to the flow rate at inlet are shown in Figure 9 for the profiles. Due to it was determined that the NACA0012, NACA1408 and EPPLER1214 profiles multiplied the flow rate by 11 times, 6 times, and 5 times, respectively. Regarding to the results, since the geometry created based on the NACA0012 profile increases the flow rate and velocity more than the others, and provides a more stable and homogeneous air flow, acoustic analyzes were continued with NACA0012 profile in the study.

4. Optimization

The optimization study was carried out to obtain the geometric design that provides the desired target values (highest flow, highest speed, least noise) by determining the lower and upper values for the geometric parameters given in Table 2.

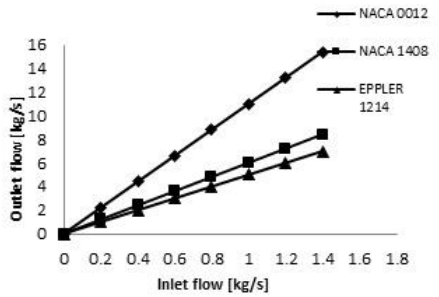

Figure 9. Rates of NACA0012, NACA 1408 and EPPLER 1214 airfoil based geometries of outlet flow to inlet flow

CFD analyzes were performed with geometries between the lower and upper ranges of the design parameters as based on the NACA0012 airfoil profile by using k-ω turbulence model in ANSYS Fluent. As a result of the analysis, it was also calculated how the design parameters in the range changed the target values.

A volumetric flow rate of 0.02 m^3/s is required at the fan inlet, and it is expected that the approximate air flow rate at the outlet will increase by 15 times (Table 3.). Air inlet velocity is calculated as 1.89 m/s for the multiplier air inlet area.

Because the diameter of the air inlet is one of the design parameter values, the change in diameter causes the velocity of the inlet air to change. For this reason, the input velocity was defined as a parameter. Outlet pressure is 0 Pa, turbulence model is k-ω.

Table 4. shows the lower and upper limit values of the design parameters. The lower and upper values were determined by taking care not to cause any distortion in the geometry when the value of any parameter is changed.

Response surface methodology (RSM) is a collection of mathematical and statistical techniques, which was applied to establish a mathematical model between independent variable and dependent variable, and find the effect of parameters affecting a response in a process [17]. Originally, RSM was developed to model experimental responses and then migrated to the modelling of numerical experiments.

Table 3. Expected value as a result of calculation

Air inlet volume flow	Air outlet volume flow
0.02 m^3/s	0.3 m^3/s

Table 4. Parameter values

Parameters	Lower values	Upper Values
Width [mm]	8	12
Angle of attack [°]	0	20
Gap [mm]	2	10
Diameter [mm]	110	130
Tail length [mm]	7	15
Tail angle [°]	30	60
Length [mm]	180	220

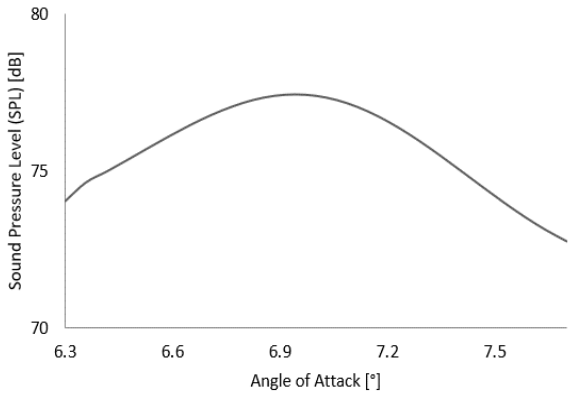

(a)

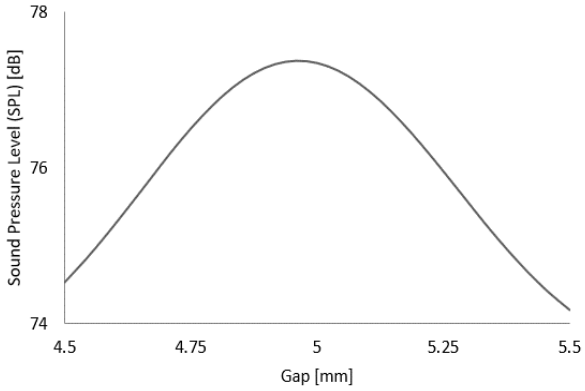

(b)

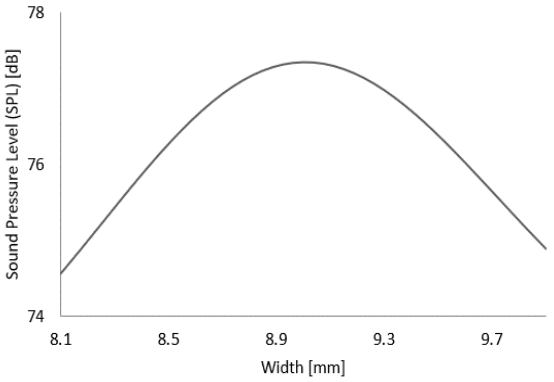

(c)

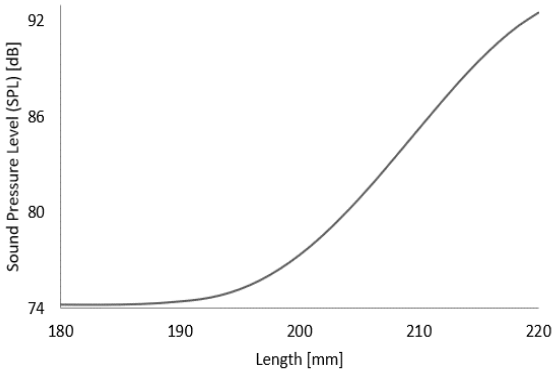

(d)

The Response Surface Optimization method allows us to determine how the parameters change the target values in the specified ranges and to perform the optimization by determining the design parameter values that provide the desired target value. The Response Surface Optimization module was connected to the Fluent analysis and the targets was selected the minimum noise-and maximum flow rate.

The changes in sound pressure caused by the change of each parameter are given in Figure 10. Other parameters were kept constant at the values indicated in Table 2 while examining the changes. As can be seen in Figure 10.a, the sound pressure level increased parabolically from 6.3° to 6.94° of angle attack and reached the maximum sound pressure level of 77 dB, then the sound level decreased parabolically with from 7° to 7.7° of angle attack. As can be seen in Figure 10.b, The sound pressure increased linearly until the gap value was 4,8 mm, and at 5 mm it reached the highest sound pressure level of 77 dB. Although the gap value increased, the sound pressure level decreased linearly. The sound pressure level increased linearly up to the value of the width parameter was 8,8 mm, reaching the highest sound pressure level of 77 dB at 9 mm of. While the width value increased, the sound pressure level decreased linearly (Figure 10.c). As can be seen Figure 10.d, while the value of the length parameter was 195 mm and above, the sound pressure level increased linearly. It reached the highest sound pressure level of 92 dB at 220 mm.

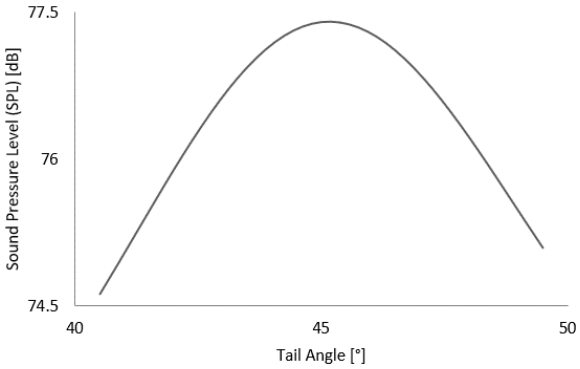

(e)

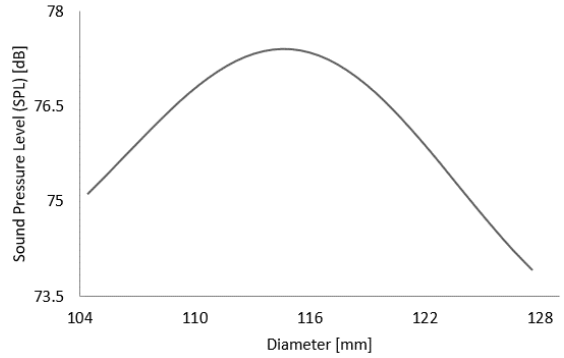

(f)

Figure 10. Effect of design parameters of NACA 0012 on sound level (a) Angle of attack (b) gap (c) width (d) length (e) tail angle (f) diameter

As can be seen Figure 10.e, the sound pressure level increased linearly up to the value of the tail angle parameter was 44°, and the highest sound pressure level reached 77 dB at 45°. In the following values, although the value of the tail angle increased, the sound pressure level decreased linearly. As can be seen Figure 10.f, the sound pressure level increased linearly up to the value of the diameter parameter was 103 mm, and reached the highest sound pressure level of 77 dB at 115.03 mm. While the diameter increased, the sound pressure level decreased linearly.

Optimization results made with Multi Objective Genetic Algorithm (MOGA) method on ANSYS with the help of response surface data created with RSM are given in Table 5. Three different optimal design points, P1, P2 and P3, which provide the highest the ratio of the output flow rate to the flow rate suctioned into the body by the radial fan (multiplied flow rate) and lowest sound pressure level targets, and the values of the design parameters at these points are given in the Table 5.

Table 5. Optimization results

Parameters	P1	P2	P3
Width [mm]	9.8193	9.8678	9.8968
The angle of Attack [°]	7.6962	7.6769	7.6848
Gap [mm]	5.4976	5.4898	5.4975
Diameter [mm]	115.21	115.93	112.73
Tail length [mm]	9.3284	9.3161	9.5405
Tail angle [°]	42.801	42.984	42.396
Length [mm]	201.74	199.12	199.14
Ratio of flow rates	4.437	4.4831	4.5213
Sound pressure level [dB]	84	84	84

4.1 Calculation of Sound Pressure Level with k-ω Turbulence Model

A mesh structure has been created for the geometry that produces the least noise and corresponds to the highest ratio of flow rates. The k-ω method yields more accurate results in boundary layer calculations. Moreover, in calculations of acoustic pressure variation, the k-ω method is more suitable for calculating tonal noise. Time dependent flow field analyzes were performed using k-ω turbulence model and Ffowcs William-Hawkings (FW-H) acoustic analogy approach with ANSYS Fluent.

Reference microphones are placed on the geometry in order to examine the sound pressure distribution results. The locations of the microphone points are given in Figure 11. Figure 12 shows the values obtained from the microphones at the reference points at different frequencies.

Table 6. shows the sound pressure level at the microphone points. The 6th and 7th points are in the gap region where the fluid in the body comes out. Since the air velocity is high and the pressure is low here, the air at stagnant atmospheric pressure behind the body moves towards this low pressure region. Therefore, eddies are formed in this region and noise increases for high frequency values. A decrease of approximately 30 dB was observed in the noise level of the microphones at the 4th point, where located just at the exit of the body, and the 5th point, where located more distance of outlet of body. The lowest noise level was calculated as 90 dB at the 5th point.The noise value measured at the 2nd point 50 mm behind the body in the air flow direction is lower than the value at the 1st point, which is the starting point of the body. The noise level at the microphones at point 8 and point 9, which are inside the body but further upstream of the output gap, have a lower value than those at points 6 and 7.

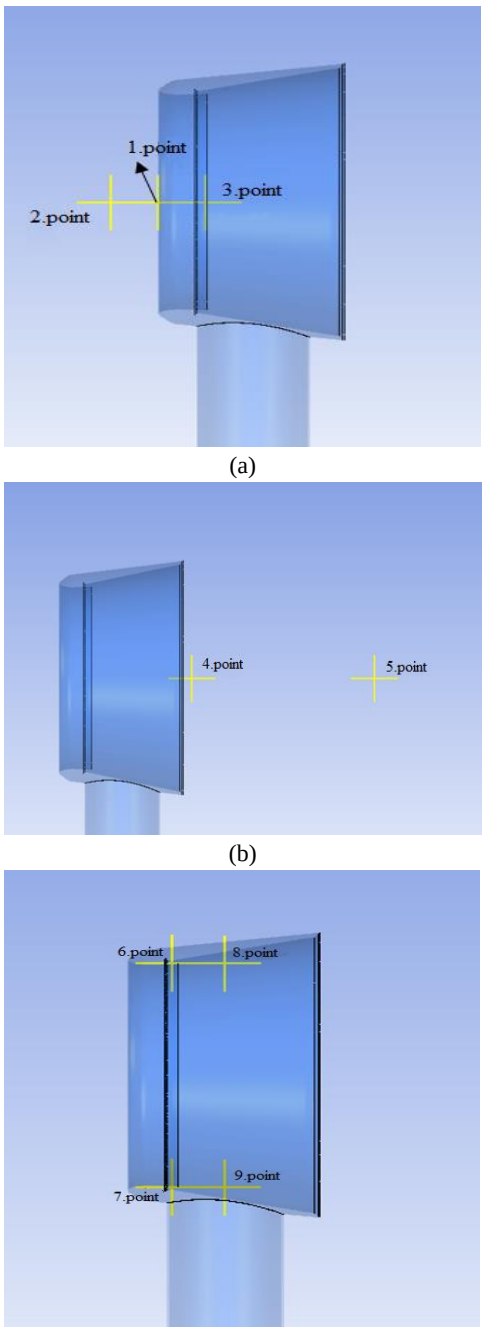

Figure 11. Microphone points of the NACA 0012 airfoil k-w turbulence model (a) 1.point, 2.point and 3.point, (b) 4.point and 5.point, (c) 6.point, 7.point, 8.point and 9.point

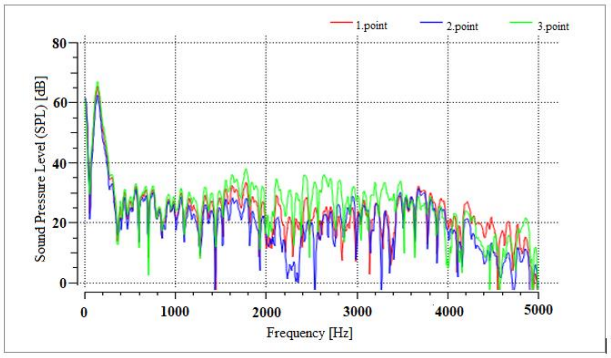

(a)

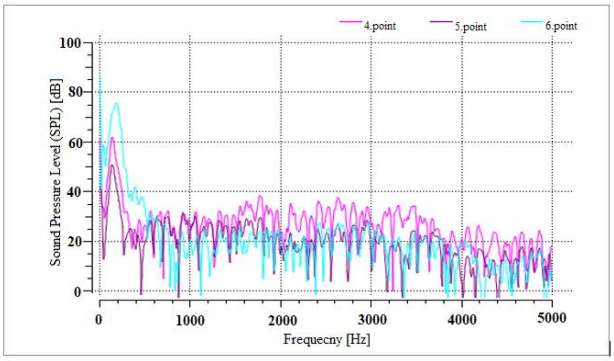

(b)

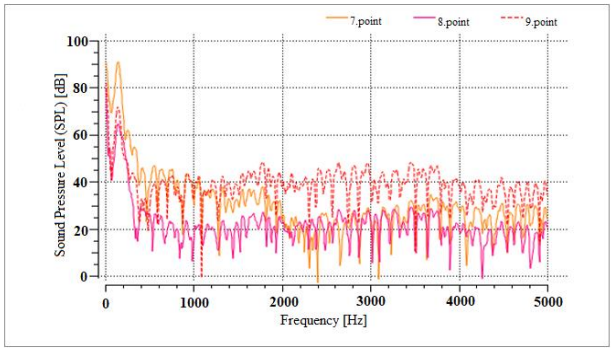

(c)

Şekil 12. According to the k-w turbulence model For 1.point, 2.point and 3.point, (a) 4.point,5.point and 6.point (b) 7.point, 8.point and 9.point (c) The effect of frequency on sound pressure level of points

Table 6. Sound pressure level

Points	Sound Pressure Level (dB)
1.point [mm]	97 dB
2.point [mm]	94 dB
3.point [mm]	98 dB
4.point [mm]	95 dB
5.point [mm]	90 dB
6.point [mm]	110 dB
7.point [mm]	120 dB
8.point [mm]	97 dB
9.point [mm]	105 dB

Sudden changes in the sound pressure level at high frequency values are due to the effect of eddy regions caused by pressure changes. Since the eddy represents the high energy in the flow field, the change in high frequencies increases the noise level due to the eddies.

4.2 Calculation of Sound Pressure Level with LES Model

Using LES turbulence model instead of the k-ω turbulence model in computational fluid dynamics allows to obtain more accurate solutions [10]. With models such as LES, large-scale eddy structures in the flow can be solved with the help of additional models (such as WALE Subgrid Scale, and Smagorinsky Subgrid Scale models), and the turbulence behavior can be solved mathematically at a rate of 90% directly [10]. Time dependent flow field analyzes were performed using LES turbulence model and FW-H acoustic analogy approach with ANSYS Fluent.

Figure 13 shows the values obtained from the microphones at the reference points at different frequencies.

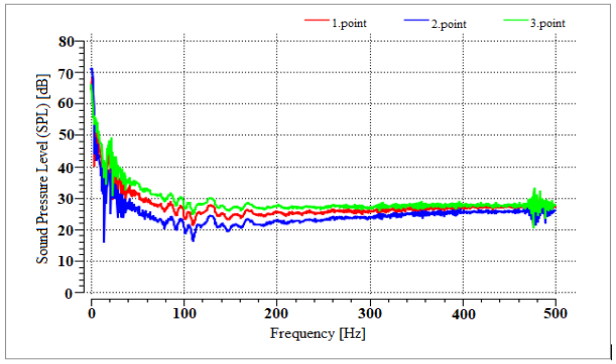

(a)

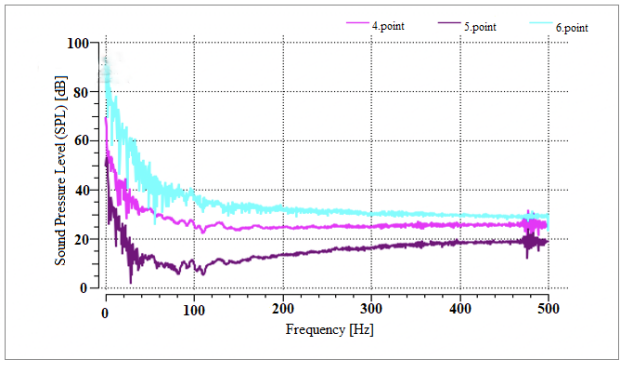

(b)

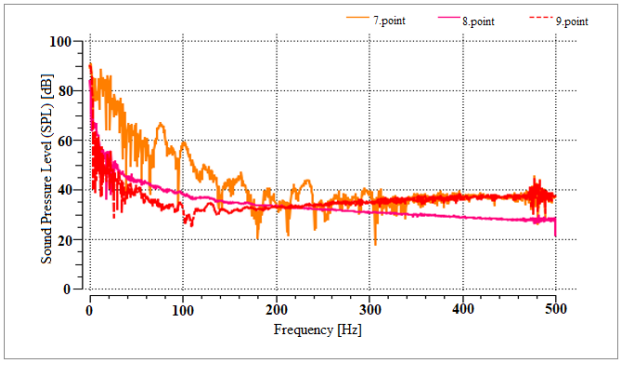

(c)

Figure 13 For the LES turbulence model, For 1.point, 2.point and 3.point, (a) for 4.point,5.point and 6.point (b) for 7.point, 8.point and 9.point (c) The effect of frequency on sound pressure level

Table 7. Sound Pressure Levels

Points	Sound Pressure Levels (dB)
1.point [mm]	70 dB
2.point [mm]	66 dB
3.point [mm]	72 dB
4.point [mm]	71 dB
5.point [mm]	57 dB
6.point [mm]	93 dB
7.point [mm]	98 dB
8.point [mm]	84 dB
9.point [mm]	81 dB

Table 7. demonstrates the sound pressure level at the microphone points. At 6th and 7th points, since air around the profile body has moved towards the low-pressure region, eddies have formed. According to the LES model calculation results; at the 6th and 7th points, the noise increased for high-frequency values. The noise level of the microphones at the 4th and 5th points showed a decrease of approximately 20 dB and 40 dB, respectively, from the noise levels at the 6th and 7th points. The lowest noise level was calculated as 57 dB at the 5th point. The value measured at the 2nd point has a lower noise value than the 1st point. As seen in microphones at 8th and 9th points, the velocity has a lower value compared to points 6 and 7. Therefore, the noise level has been reduced by about 13 dB. The rapid changes seen in the sound pressure level data at high-frequency values are due to the effect of pressure drops and eddy zones.

The results obtained from the calculations with k-ω at the 6th and 7th points, 22 dB higher sound pressure level was measured than the values calculated with the LES. The results obtained from the calculations with k-ω at the 1st point and the 2nd point, 28 dB higher sound pressure level was measured compared to the values calculated with the LES. The lowest sound pressure level was calculated at the 5th point in the solution with the k-ω turbulence model and LES model, and the results obtained from the calculation with the LES are 33 dB lower than the noise value calculated with the k-ω turbulence model. Points 4 and 5 are two points outside the air multiplier fan. The noise difference between calculations with the k-ω turbulence model and LES model is 24 dB at 4th point, and is 33 dB at 5th point, and is 26 dB at 3th point.

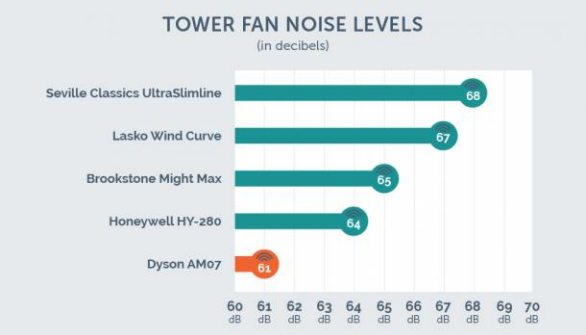

Figure 14. Fan Noise Level by Dyson company [2]

The results obtained with the LES method are more sensitive than the results calculated with the k-ω turbulence model. However, the solution time is longer. While the k-ω method solves turbulence by modeling, LES provides a direct solution. Therefore, the results of the calculations using the LES method are closer to the noise results announced by the Dyson company (Figure 14).

5. Conclusions

In this stud, three different air multiplier fan geometries were created based on NACA 0012, NACA1408, and EPPLER 1214 airfoils. As a result of the calculations made with CFD analysis, it was determined that the body profile providing the highest flow rate was NACA 0012. Using the ANSYS Response Surface optimization tool with seven geometric design parameters, a CFD-based study was conducted to determine the design that generates the least noise against the ratio of flow rate.

In the design that produces the least noise, the ratio of the output flow to the input flow is calculated as approximately 4.5. The geometry with the body profile of the bladeless fan determined as a result of this optimization was calculated using CFD analyzes and sound pressure level k-ω and LES turbulence models.

According to the results of these calculations, the noise decreases as the gap parameter value increases, the noise decreases as the angle of attack parameter value increases, the noise decreases as the width parameter value increases, the noise decreases up to a certain value of the length parameter value increases, then it has a constant value. The tail angle value increases, the noise decreases up to the 45º of the value of the parameter. As the diameter parameter increases, the noise decreases parabolically. When the value of the tail length parameter is up to 9 mm, the noise decreases and then increases.

By using the k-ω and LES method, the pressure distribution over 9 different microphones (observation) points were examined depending on time. It has been observed that the results obtained from the solutions made with the LES method are more sensitive and closer to the results announced by the Dyson company. The results obtained with the LES method showed that the determined design was usable.

Declaration

The authors declared no potential conflicts of interest with respect to the research, authorship, and/or publication of this article. The authors also declared that this article is original, was prepared in accordance with international publication and research ethics, and ethical committee permission or any special permission is not required.

Author Contributions

F. Yedekcioglu developed the methodology. S. Akyildiz performed the analysis. Z. Parlak supervised and improved the study. All authors wrote the manuscript together.

References

1. Bleier, F. P., *Fan Handbook: Selection, Application and Desing*. 1998, USA: McGraw-Hill.
2. Dyson UK. [cited 2020 20 June]; Available from: https://youtu.be/gChp0Cy33eY/.
3. Li, G., Hu, Y., Jin, Y., Setoguchi, T., and Kim, H. D., *Influence of Coanda surface curvature on performance of bladeless fan*. Journal of thermal science, 2014. **23**(5): p. 422-431.
4. Lasse, C. H., and Simon, H. T., *Flow Characteristics of the Dyson Air Multiplier*. Semantic Scholar, 2014. **14(**7).
5. Li, H., Deng, H. S., & Lai, Y. B., *Numerical and experimental research on the outlet flow field for the air multiplier*. Applied Thermal Engineering, 2016. **93**: p. 652-659.
6. Jafari, M., Afshin, H., Farhanieh, B., & Sojoudi, A., *Numerical investigation of geometric parameter effects on the aerodynamic performance of a Bladeless fan*. Alexandria Engineering Journal, 2016. **55(**1): p. 223-233
7. Zafer, B., Gürsoy, S., *Üflemeli kontrol sistemine sahip kanat kesitinin aeroakustik incelenmesi*. Uludağ Üniversitesi Mühendislik Fakültesi Dergisi, 2016. **21(**2): p. 237-256..
8. E. Kocak., E. Ayli., H.Turkoglu, *Kanat profili - silindir konfigürasyonunun aerodinamik ve aeroakustik performansinin sayisal analizi, in* 14th Ulusal Tesisat Mühendisliği Kongresi. 2019. İzmir: p. 908-917
9. İlter, Y.K., *İki Boyutlu Cisimler Etrafındaki Akım Gürültüsünün İncelenmesi*. 2014, İstanbul Teknik Üniversitesi, Fen Bilimleri Enstitüsü, Gemi İnşaatı ve Gemi Makinaları Mühendisliği Anabilim Dalı, Yüksek Lisans Tezi.
10. A.Bacak., A. Pinarbasi *Eksenel fan akustik performansinin sayisal olarak incelenmesi*, in 4th Uluslararasi Katilimli Anadolu Enerji Sempozyumu. 18-20 Nisan 2018. Edirne: p 798-804.
11. Li, A., *Characterization of Aerodynamic and Aeroacoustic Performance of Bladeless Fans*. 2019, Doctoral dissertation, Purdue University Graduate School.
12. Mehmood, K., Shahzad, A., Masud, J., Akram, F., Mumtaz, M. N., & Shams, T. A., *Numerical analysis of bladeless ceiling fan: An effective alternative to conventional ceiling fan*. Journal of Wind Engineering and Industrial Aerodynamics, 2022. **221**: 104905.
13. Ravi, D., & Rajagopal, T. K. R., *Numerical investigation on the effect of geometric shape and outlet angle of a bladeless fan for flow optimization using CFD techniques*. International Journal of Thermofluids, 2022. **15:** 100174.
14. Jafari, M., Sojoudi, A., & Hafezisefat, P., *Numerical study of aeroacoustic sound on performance of bladeless fan*. Chinese Journal of Mechanical Engineering, 2017. **30**(2): p. 483-494.
15. Li, H., Jin, X. H., Deng, H. S., & Lai, Y. B., *Experimental investigation on the outlet flow field structure and the influence of Reynolds number on the outlet flow field for a bladeless fan*. Applied Thermal Engineering, 2016. **100**: p. 972-978.
16. Joshi, V.; Noronha, W.; G, V.; Ramasamy, S.; K B, R. *Determination of Optimum Outlet Slit Thickness and Outlet Angle for the Bladeless Fan Using CFD*. Preprints, 2022. **2022110459**: p 1-17
17. Zhou, J., Hatami, M., Song, D., & Jing, D., *Design of microchannel heat sink with wavy channel and its time-efficient optimization with combined RSM and FVM methods*. International Journal of Heat and Mass Transfer, 2016. **103**: p. 715-724..